New Journal of Physics
The open-access journal for physics

Tunable diode laser absorption spectroscopy of argon metastable atoms in Ar/C_2H_2 dusty plasmas

Hoang Tung Do[1], **Vladimir Sushkov and Rainer Hippler**
Institut für Physik, Ernst-Moritz-Arndt-Universität Greifswald,
Felix-Hausdorff-Strasse 6, 17489 Greifswald, Germany
E-mail: do@physik.uni-greifswald.de

New Journal of Physics **11** (2009) 033020 (16pp)
Received 5 December 2008
Published 13 March 2009
Online at http://www.njp.org/
doi:10.1088/1367-2630/11/3/033020

Abstract. The tunable diode laser absorption spectroscopy method was used to measure Ar metastable density in order to study the dust growth process in hydrocarbon-containing plasmas. A simple model was proposed that successfully interprets the experimental results of pristine plasmas. The model is also suitable for explaining the influence of dust particle size on metastable density and for examining the dust growth process. The metastable density responded strictly to the formation of dust particles and their growth in processing plasmas. Using metastable density as an indicator is, therefore, a non-intrusive and effective method for the study of the dust growth process in hydrocarbon-containing plasmas.

[1] Author to whom any correspondence should be addressed.

Contents

1. Introduction

The interest in plasma–particle interactions in dusty plasmas has grown enormously during the last decade [1, 2]. The increased interest was mainly caused by applied research related to materials science [3]–[5] and, recently, also with regard to plasma diagnostics [6]–[8]. Powder formation has been a critical concern for the microelectronics industry, because dust contamination can severely reduce the yield and performance of fabricated devices. Submicron particles deposited on the surface of process wafers can obscure device regions, cause voids and dislocations and reduce the adhesion of thin films [9, 10].

In hydrocarbon-containing plasmas, a large amount of dust particles is effectively and continuously created and trapped inside the plasma. Dust particle size and density can reach significant values resulting in a recognizable decrease of transmitted laser light and a remarkable increase of scattered laser light [11]. A dust void is subsequently created at the center of the dust cloud under the action of the ion drag force [12], which becomes significant once the dust particle size and density reach critical values. Meanwhile, a new dust generation forms in the free space. The new generation grows both in size and number density until it is also pushed out.

The growth process of dust generation in a chemically reactive plasma can be divided into three steps [10, 13]: nucleation, agglomeration and accretion. In the nucleation phase, the (sub)nanometer-sized protoparticles are formed as a result of homogeneous or heterogeneous processes. Later in the agglomeration step, these protoparticulates, after reaching a critical density, merge together, forming particles with sizes of a few per tens of nanometers. The particles of this size quickly acquire a negative electric charge by ion and electron collection, which requires the plasma to reorganize. In order to compensate the electron losses, the effective electron temperature increases [14] resulting in an increase of ionization and excitation. This reorganization of the plasma is called the α–γ' transition [15]. After this transition the particles accrete neutral and ionic monomers to grow into larger particles until all of them are driven away. The accretion process is relatively slow, and no new particle is formed in the accreting dust cloud. The time evolution of the dust growth, therefore, is parameterized by three characteristic times: T_{trans}—the time the processing plasma needs to reach the α–γ' transition;

T_{void}—the time for the appearance of the dust void; and T_p—the growth period of one dust generation.

Tunable diode laser absorption spectroscopy (TDLAS) can support the optimization of industrial plasma processes by permitting highly specific, accurate, and non-intrusive real-time monitoring of species densities. TDLAS offers significant advantages compared with conventional spectroscopy. The spectral width of the laser radiation (a few megahertzs) is much smaller than the width (a few gigahertzs) of the Doppler-broadened absorption profile. The sensitivity and the signal-to-noise ratio are also increased in TDLAS due to the use of a high-power coherent source. The high sensitivity gives TDLAS the ability to detect and measure gas temperature and low concentrations. For example, such measurements have been successfully shown during Al sputtering from a magnetron discharge [17, 18]. Moreover, an advantage of TDLAS in studying dusty plasma is that the presence of dust particles does not influence the metastable density measurement. The scattering and absorption effects can be taken out from the intensity profile.

The metastable density is an important plasma parameter. The metastable atoms are abundant and energetic. So far, the role and effects of metastable atoms in dusty plasmas have not been considered to a large extent, especially in the formation and growth of dust particles in processing plasmas. There has been a lack of consideration of these species in such a plasma environment. In the present paper, we study the influence of dust particle size and density on argon metastable density. Metastable density, consequently, will be used as an indicator to investigate the dust growth process in hydrocarbon-containing plasmas.

2. Experimental set-up

The experiments were performed in the PULVA reactor (figure 1) [19]–[22]. It consists of a vacuum chamber of 40 cm diameter. Two caps each with a small slit (2 mm × 30 mm) were used to decrease the absorption length to 25 cm in order to avoid saturation of the absorption line. A typical absorption spectrum, together with the etalon signal, is displayed in the inset of figure 1. The chamber is pumped by a turbo molecular pump with a pumping speed of 260 liters s^{-1}, which is backed by a membrane pump. The residual gas pressure is 10^{-4} Pa. An adjustable butterfly valve is mounted between the pump and the chamber. Working gases are introduced into the vacuum chamber by two separate flow controllers. As the process gas, an argon/acetylene gas mixture was used. The discharge was driven at 13.56 MHz by a radio frequency (rf) generator coupled to the bottom electrode by a matching network. The bottom electrode has a diameter of 13 cm and is situated near the center of the chamber; the chamber wall serves as the other electrode. Measurements were carried out at working pressures of 1–15 Pa and at rf powers of 1–60 W. The typical electron temperature and the density of pure Ar plasma are 2 eV and 2×10^{15} m^{-3} (at 10 W), respectively [23, 24].

The laser system consists of a tunable single-mode diode laser and a control unit for diode temperature and diode current (Toptica DL 100). The diode laser utilizes an extended cavity laser set-up with optical feedback into the laser diode from the first order of a spectrally selective grating. The laser light traverses a polarization filter and is directed to a beam splitter. The transmitted light is registered by a photo diode behind a Fabry–Perot etalon to monitor the light frequency [17]. The second light beam traverses the plasma chamber and is detected by a second photodiode.

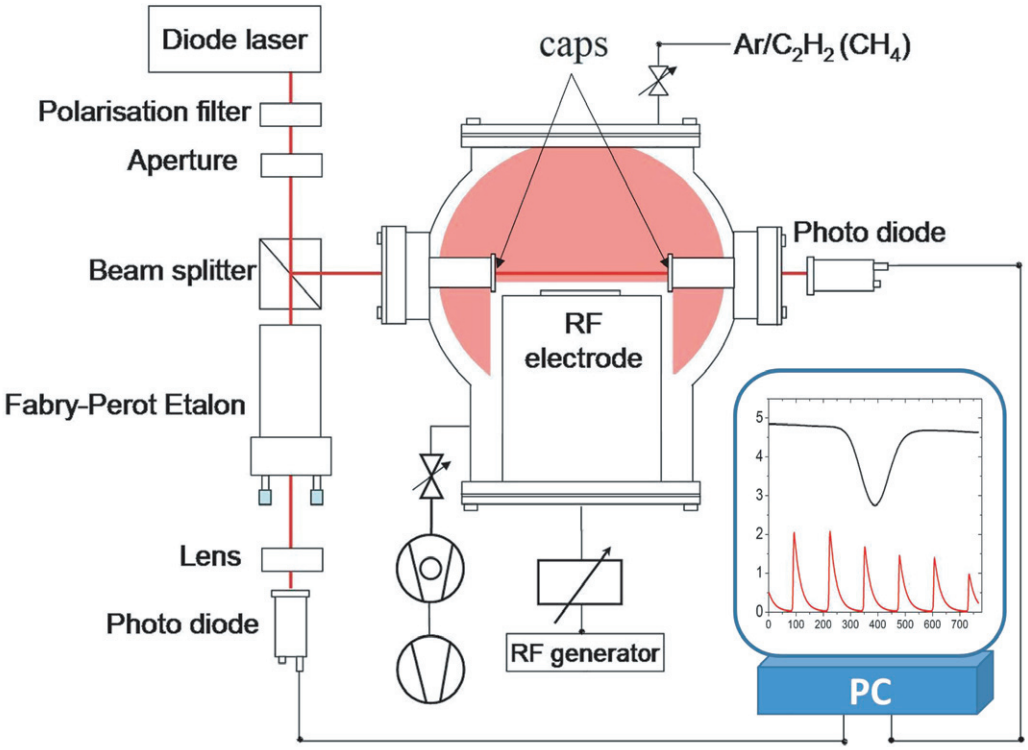

Figure 1. Experimental set-up (schematic). The inset shows a typical absorption spectrum (upper curve) together with the etalon signal (lower curve).

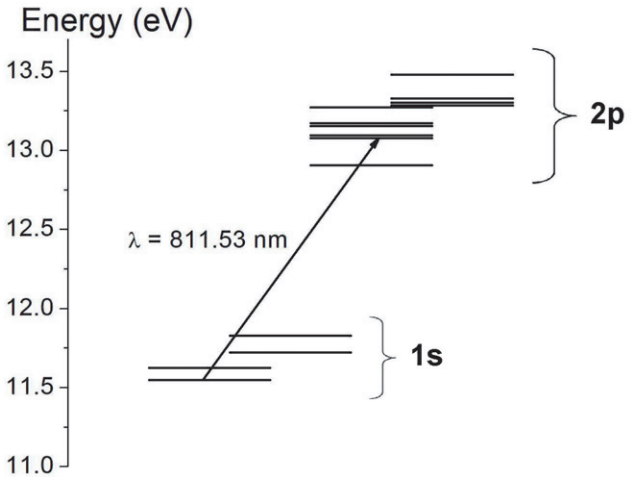

Figure 2. Argon term diagram of the 1s and 2p levels (in Paschen's notation). Energy values were taken from the NIST database [16].

Without plasma, the laser intensity, as measured by the second photodiode, linearly increases. In the case of a burning discharge, the photodiode signal shows pronounced variations in the neighborhood of a wavelength of 811.53 nm due to absorption by excited argon atoms (see figure 2). The transmitted intensity follows the Lambert–Beer law of absorption. Under the assumption of a constant Ar density inside the plasma region, and the Doppler broadening of

the absorption line, the atom density n_m is related to the integrated absorption profile $\kappa(\nu)$ [26]

$$n_m = \frac{4\pi\varepsilon_0 m_e c}{e_0^2 f \lambda_0}\sqrt{\frac{2kT}{\pi m_a}}\kappa_0, \tag{1}$$

where κ_0 is the absorption coefficient in the center of the profile, ε_0 is the dielectric constant, c is the speed of light, m_e and e_0 are the electron mass and charge, respectively, m_a is the atomic mass of Ar, k is the Boltzmann constant, $\lambda_0 = 811.53$ nm is the central wavelength of the investigated transition and f is the optical oscillator strength for the investigated transition. The width of the absorption signal is related to the temperature T of Ar atoms by the equation

$$T = \frac{\lambda_0^2 m_a}{8k \ln 2}\Delta\nu^2, \tag{2}$$

where $\Delta\nu$ is the effective full-width at half-maximum of the measured absorption profile.

An advantage of metastable argon is that argon essentially consists of ^{40}Ar isotope (99.6%) with zero magnetic momentum; therefore the transmitted photodiode signal can be fitted by a Doppler profile. A least-squares fit was used to analyze the data. The fit quality was excellent with deviations, on a point-to-point comparison, of less than 1%. The accuracy of the obtained atom density derived via equation (1) is essentially determined by the estimated accuracy of the underlying oscillator strength f of ±25%, an estimated accuracy of the absorption length inside the plasma of 5% and a negligible statistical uncertainty of less than 0.1%, adding up to an estimated overall accuracy for the absolute mean argon atom density of about ±25%.

3. Metastable density

3.1. Metastable density in pristine argon plasma and the quantitative treatment

The dependence of the argon metastable atom number density n_m on the input rf power has been obtained experimentally in a pure argon discharge (see figure 3). As can be seen, the metastable density monotonically increases with power with a tendency to saturate before 50 W.

The behavior of the metastable atoms can be explained in the framework of a simple model. We use the balance equation for the metastable atoms:

$$\frac{\partial n_m(t)}{\partial t} = \sum_i G_i - \sum_j L_j, \tag{3}$$

where G_i are the rates of different production processes and L_j are the rates of losses. The spatial distribution of metastables is not uniform, and in our case n_m is a 'line-of-sight'-averaged quantity.

As long as we are interested in a stationary solution ($\partial n_m/\partial t = 0$), the balance equation can be solved algebraically with respect to n_m. The production channels are independent of the density of metastables. Most of the loss rates are proportional to n_m, i.e. $L_j = n_m \nu_j$, where ν_j is the frequency of the corresponding loss channel. The diffusion is also represented in this linear form, assuming that the coefficient of excitation energy accommodation on surfaces equals 1.

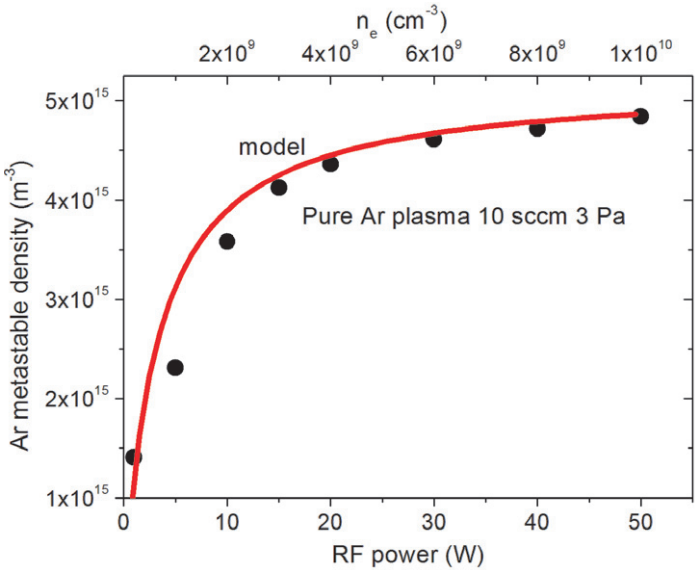

Figure 3. Input power dependence of metastable density in an rf discharge in comparison with model calculation.

Metastable pooling, an essentially nonlinear loss channel, is negligible in our conditions. Thus, the solution to equation (3) is given as

$$n_{\mathrm{m}} = \frac{\sum_i G_i}{\sum_j \nu_j}. \tag{4}$$

Among the numerous channels leading to population and depopulation of the metastable level, the radiative–collisional coupling to other excited states (for the most part to 1s- and 2p-states) is difficult to accurately take into account. For this purpose, the whole system of balance equations for all excited states should be solved. But the low-temperature, low-pressure conditions, which we have, allow us to make a simplifying assumption concerning the role of the excited states. We assume that their densities are small and do not contribute to the population of metastables. The metastable atoms are quenched by electron impact to radiative 1s-states with a rate constant $k_{\mathrm{quench}} = 2 \times 10^{-7}\ \mathrm{cm}^3\ \mathrm{s}^{-1}$, widely accepted in the literature [27, 28]. Collisions with electrons can also excite metastables into 2p-levels; the rate constant for this channel is estimated to be of about the same value $k^{\mathrm{m}}_{\mathrm{exc}} = 2 \times 10^{-7}\ \mathrm{cm}^3\ \mathrm{s}^{-1}$, which is consistent with the data in [27, 29].

The frequency of diffusion loss (de-excitation due to collisions with walls) is accounted for by the term $D_{\mathrm{m}}/l^2_{\mathrm{eff}}$, where $D_{\mathrm{m}} = 3.3 \times 10^3\ \mathrm{cm}^2\ \mathrm{s}^{-1}$ [30] is the diffusion coefficient of metastable argon atoms in the parent gas at 3 Pa, and l_{eff} is the effective diffusion length.

We may drop the terms accounting for losses in two- and three-body collisions with background atoms, since they start to play a role at pressures at least one order of magnitude higher [31].

The final result describing the dependence of n_{m} on plasma parameters is obtained as

$$n_{\mathrm{m}} = \frac{k_{\mathrm{exc}} n_{\mathrm{g}} n_{\mathrm{e}}}{D_{\mathrm{m}}/l^2_{\mathrm{eff}} + (k_{\mathrm{quench}} + k^{\mathrm{m}}_{\mathrm{exc}}) n_{\mathrm{e}}}, \tag{5}$$

where n_g is the ground state density, n_e the plasma density and k_{exc} the rate coefficient for the ground state excitation into the metastable level. k_{exc} is defined as usual as a product of electron velocity and cross section, averaged over the velocity electron distribution function (EDF). We take the cross section for ground state excitation from the work [32], and take an average over a Maxwellian EDF. As a result, we get $k_{exc}(T_e^{eff})$ as a function of the effective electron temperature T_e^{eff}.

With equation (5) we got a plasma density dependence of metastables. Now let us take advantage of the fact that in low-pressure CCP discharges n_e is to a great extent proportional to input power P, whereas the mean electron energy does not change with power. This fact allows us to formulate a relation between power and plasma density scales $n_e = kP$, with the proportionality coefficient $k = 2 \times 10^8\,\mathrm{cm^{-3}\,W^{-1}}$ [23].

Finally, we have two fitting parameters T_e^{eff} and l_{eff} for the experimental curve. A good fit to the experimental data yields the values $T_{e0}^{eff} = 1.8\,\mathrm{eV}$ and $l_{eff} = 3.0\,\mathrm{cm}$ (see figure 3).

It is a well-established fact in the literature that for the low-pressure case of CCP discharge the EDF is bi-Maxwellian. The majority of electrons have a temperature in the range of 0.3–1 eV, and 10–20% have a temperature in the range of 3–4 eV (see, for example, [23, 34, 35]). Thus, the value of $T_{e0}^{eff} = 1.8\,\mathrm{eV}$ appears reasonable. The value of l_{eff} is also realistic for our geometry. (In the case of pure spherical or cylindrical geometry $l_{eff} = R_r/\pi$ or $l_{eff} = R_r/2.4$, where R_r is the corresponding radius.)

The input power dependence of argon metastable number density can be understood as follows. At low powers the diffusion losses are dominated by diffusion and n_m rises almost linearly (with power or plasma density). Then the losses through electron collisions take over, and at higher powers n_m tends to a constant value. In between there is a transition region, where both loss channels play an equally important role.

3.2. Time evolution of metastable density in hydrocarbon-containing plasma

Similar to small molecular ions [11], the temporal behavior of metastable density also follows the periodic variation of the plasma as well as particle density and size. As can be seen in figure 4, the metastable density drops instantly when C_2H_2 is inserted due to the reactions between metastable atoms and the processing gas, producing reactive radicals that ignite the neutral growth channel of dust particles [33]:

$$C_2H_2 + Ar^* \rightarrow C_2H + H + Ar. \tag{6}$$

$$C_2H + Ar^* \rightarrow C_2 + H + Ar. \tag{7}$$

The formed radicals further react with C_2H_2 to form larger radicals, e.g.

$$C_2H + C_2H_2 \rightarrow C_4H + H_2 \tag{8}$$

and

$$C_2 + C_2H_2 \rightarrow C_4 + H_2 \tag{9}$$

and so forth. Shortly after the acetylene flow is added, the metastable density drastically increases, indicating the change in plasma mode, namely a α–γ' transition. The appearance of a dust void leads to a separation of the plasma into a dust-free plasma inside the void with low metastable density and a dusty plasma with high metastable density outside. This is because

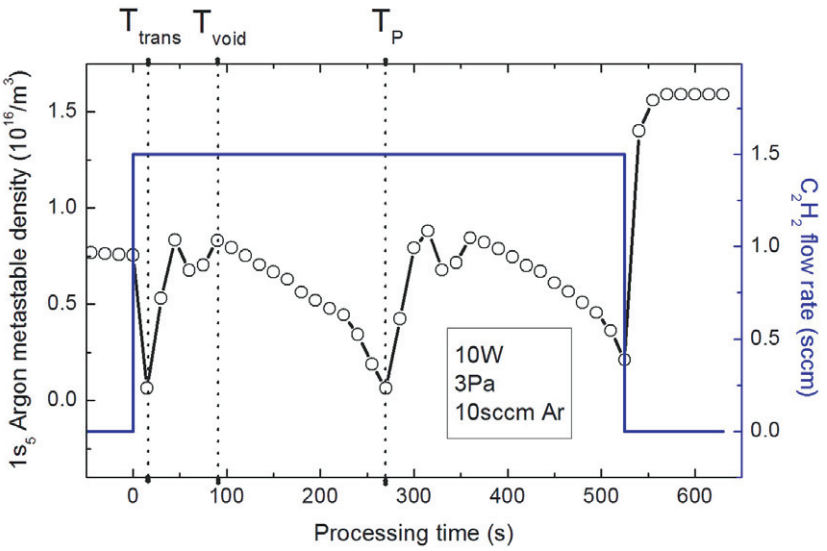

Figure 4. Time evolvement of metastable density in the processing plasma. The change in metastable density is an indication of the change in plasma parameters, especially the dust density and size.

of the high electron temperature in the dust-containing region compared with the dust-free region [37]. Therefore, the metastable density slightly decreases as the void starts to expand. At the end of the dust growth period, when the outer dust cloud is pushed away the metastable density drastically drops again (figure 4).

As explained above, the metastable density follows the time evolvement of the dust growth in a processing plasma. From the temporal behavior of the metastable density, we can easily define T_{trans}, T_{void} and T_{p} (see figure 4). The metastable density can be used as an indicator of the changes in the plasma, especially the electron temperature and density, as well as to trace the phase transitions in a processing plasma between: nucleation, agglomeration, accretion and dust-expelling phases.

A significant difference exists between the argon metastable densities before introducing the acetylene and after switching off the acetylene (figure 4). In the former case, we have a pure Ar plasma with low metastable density, whereas in the latter case we have dusty plasma of nanohydrocarbon particles giving rise to high metastable density.

The dust productivity of Ar/C_2H_2 plasma is so high that only slow phases like accretion and dust-expelling phases can be seen. In order to get insights into the nucleation phase, an Ar/CH_4 rf plasma was employed to extend T_{trans}. The evolvement of metastable density in this transient time can be visualized. In the nucleation phase, there exists a period where the metastable density slightly increases (marked by a red circle in figure 5). The increase in metastable density from 1.8×10^{14} to $2.2 \times 10^{14}\,\text{m}^{-3}$($\sim$25%) is small compared with the change at the α–γ' transition, but in fact cannot be neglected. In the nucleation phase, we have a particle balance for metastables between the direct excitation by electrons, the loss by electron collision, the loss by diffusion and the loss by reaction with hydrocarbon species. At this plasma stage, the hydrocarbon species are growing and accumulating more and more in the plasma. Therefore the loss of metastables in reactions with hydrocarbon species should generally increase, which results in about 60 s decrease of metastable density in the first half of the nucleation phase.

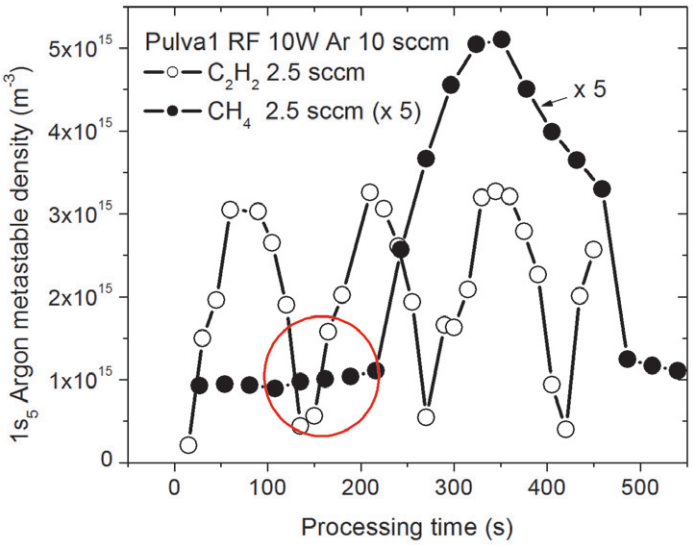

Figure 5. Time evolvement of metastable density in Ar/C_2H_2 (○) and Ar/CH_4 (●) rf plasmas. The dust productivity of the Ar/C_2H_2 plasma is higher than that of the Ar/CH_4 plasma as the dust growth period is much shorter in the Ar/C_2H_2 plasma ($T_p = 130$ s) compared with the Ar/CH_4 plasma ($T_p = 540$ s).

Therefore, the increase of metastable density in the latter half of the nucleation phase implies a slight rise of electron temperature. This change in electron temperature can only be explained by the appearance and growth of negative ions in this plasma. The dust growth process therefore can be associated with the growth of hydrocarbon negative ions.

In order to understand dust growth and the role of metastable atoms in processing plasmas, investigations of the dependence of metastable density on the dust particle influence are therefore highly important. The results from these studies will be expressed in the following section, which focuses on the interactions between dust particles and metastable atoms in dusty plasma as well as the influence of dust particles on metastable density.

4. Influence of grown dust particles on metastable density

Normally, in a void-free dust-dense plasma, the metastable density is significantly higher than in pristine plasma (metastable density at a plasma power less than 10 W in figure 6). However, in the presence of the dust void (plasma at a power greater than 10 W), the plasma separated itself into two parts: a pristine plasma inside the void and a dusty plasma outside the dust void. The expansion of the dust void with an increase in plasma power leads to a metastable density closer and closer to the value for pristine plasma (figure 6).

Generally speaking, the presence of dust particles has both positive and negative effects on metastable density. On the one hand, dust particles collect electrons from the plasma. In order to sustain the plasma, the electron temperature has to increase. The increase of electron temperature results in an enhancement of the excitation rate of metastables. On the other hand, the dust particles also act as quenching surfaces destroying metastables [22]. Depending on the balance between these two effects that depend on dust size and density, the metastable density will be either higher in pristine plasma if the first effect is dominant or vice versa.

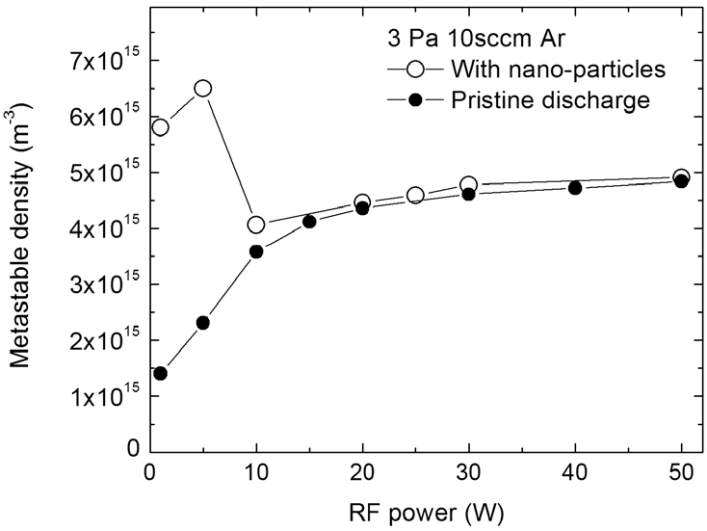

Figure 6. Metastable density in dusty (open circles) and pristine (filled circles) argon plasmas. The dusty plasma was prepared by running for 5 min a processing plasma of a 10 sccm Ar and 2.5 sccm C_2H_2 gas mixture at 10 W. When the acetylene flow was switched off, the plasma power was reduced to 1 W and then stepwise increased up to 50 W, while the metastable density was measured.

Considering equation (5) under the influence of dust particles, the effective diffusion length has to be adjusted to include the diffusion of metastables to dust particles with the corresponding effective length l_{tot} [22]:

$$\frac{1}{l_{\mathrm{tot}}^2} = \frac{1}{l_{\mathrm{eff}}^2} + \frac{1}{l_{\mathrm{D}}^2}, \tag{10}$$

where $l_{\mathrm{D}} = 1/n_{\mathrm{d}}S_{\mathrm{d}}$ is the effective length for diffusion of metastable to dust particles with n_{d} and S_{d} being the dust particle density and surface area, respectively.

The source term in equation (5) also changes due to the increase of electron effective temperature and consequently the excitation rate coefficient. Using the model in section 3 to fit the measured metastable density in dusty plasma gives a relatively high electron effective temperature, $T_{\mathrm{e}}^{\mathrm{eff}} \approx 25$ eV. This extreme temperature suggests that other excitation channels, e.g. cascade from higher levels, should play a considerable role in the metastable balance equation. Let us call the total rate of the cascade excitation $k_{\mathrm{exc}}^{\mathrm{c}}$; the metastable density in dusty plasma can be written as

$$n_{\mathrm{m}}^{\mathrm{D}} = \frac{(k_{\mathrm{exc}} + k_{\mathrm{exc}}^{\mathrm{c}})n_{\mathrm{g}}n_{\mathrm{e}}}{(1/{l_{\mathrm{eff}}}^2 + n_{\mathrm{d}}^2 S_{\mathrm{d}}^2)D_{\mathrm{m}} + (k_{\mathrm{quench}} + k_{\mathrm{exc}}^{\mathrm{m}})n_{\mathrm{e}}}. \tag{11}$$

This equation will be used to evaluate the influence of dust particle size and density later on.

4.1. The influence of dust size on metastable density

The dusty plasma with mono-dispersed grown particles was produced in an argon rf plasma in continuous mode by adding a short pulse of acetylene. The length of the C_2H_2 pulse, $\tau_{C_2H_2}$, was

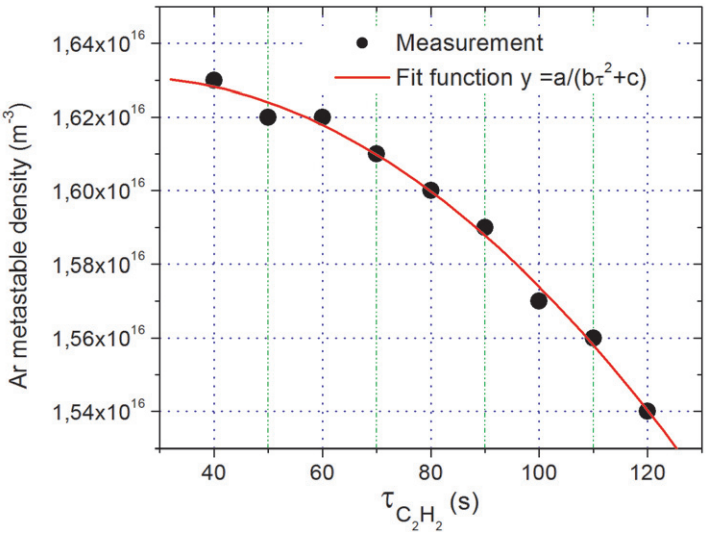

Figure 7. Metastable density of dusty plasma produced by different C_2H_2 pulse lengths.

chosen to fulfill $T_{\text{trans}} < \tau_{C_2H_2} < T_{\text{void}}$. This constraint ensures that the dust density is the same for all the chosen flow lengths, because, after the α–γ' transition, no new (or only a few more) particles were created, which guarantees that the total dust particle number remained the same. Also, there was no dust void seen, which means that the total volume occupied by dust also remains constant.

Meanwhile, longer flow length produced bigger particles. The size of particles produced by the $\tau_{C_2H_2}$ acetylene flow is more or less the same as the size of dust particles in a processing plasma at the time $t = \tau_{C_2H_2}$ after the acetylene flow was added. The dependence of dust size on the acetylene pulse length, therefore, can be regarded as the growth of dust particle size in the precessing plasma.

By comparing the metastable density of the dusty plasmas prepared by different acetylene flow lengths ($\tau_{C_2H_2}$), we obtain the relation between metastable density and dust particle size. Using equation (11), the relation between dust particle size and metastable density, in the case of constant dust density, can be expressed as the following:

$$n_{\text{m}}(\tau_{C_2H_2}) = \frac{A}{B{S_{\text{d}}}^2(\tau_{C_2H_2}) + C}, \tag{12}$$

with $A = (k_{\text{exc}} + k^{c}_{\text{exc}})n_{\text{g}}n_{\text{e}}$, $B = n_{\text{d}}^2 D_{\text{m}}$ and $C = D_{\text{m}}/l_{\text{eff}}^2 + (k_{\text{quench}} + k^{\text{m}}_{\text{exc}})n_{\text{e}}$. The metastable density in dusty plasmas produced by different acetylene flow lengths was measured and is plotted in figure 7. The dependence of metastable density on acetylene flow length can be well fitted to the function $y = c_1/(c_2\tau^2_{C_2H_2} + c_3)$. According to equation (12), the particle surface in a hydrocarbon-containing plasma after the α–γ' transition is therefore proportional to t. This result is also in agreement with the assumption we made in [11] that the product $n_{\text{d}}S_{\text{d}}$ is linearly dependent on time (n_{d} is constant in this case). Therefore the particle radius must be proportional to square root of time

$$r \propto t^{1/2}, \tag{13}$$

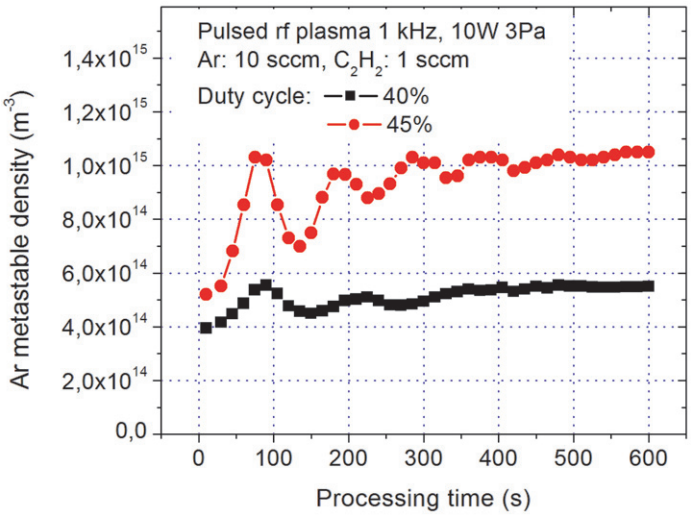

Figure 8. Metastable density of a pulsed rf plasma at different duty cycles using an Ar/C_2H_2 gas mixture. The metastable density tends to reach a steady state value, indicating an equilibrium dust density inside the plasma.

which also means

$$\frac{dr}{dt} \propto t^{-1/2}. \tag{14}$$

This particle size growth rate is a transition between ionic ($\propto t^{-2/3}$) and neutral growth (constant in time) rates [36], which suggests a combination of the two growth mechanisms in hydrocarbon-containing rf plasmas. The particle radius ($\propto t^{1/2}$) is also in agreement with the measurement of dust growth in an argon/silene plasma [38].

4.2. The influence of dust density on metastable density

It is more difficult to change the dust density of the dusty plasma generated by a processing plasma than to change the dust size. In the continuous rf plasma mode, shortly after the acetylene was turned on, the plasma is ready to proceed to the γ' mode (figure 4). The total number of dust particles does not change from then until the end of the dust generation growth.

We therefore employed pulsed rf plasmas to create plasmas of different dust densities. The dust density in a pulsed rf plasma is determined by its dust-confining ability. As can be seen in figure 8, after a certain time the metastable density in a pulsed rf plasma reaches the steady state value, implying that the dust density in this plasma also reached the equilibrium value. Consider the balance equation for dust particles

$$\frac{\partial n_d(t)}{\partial t} = G_d - L_d. \tag{15}$$

The density of the dust confined in a pulsed plasma, besides the plasma power, depends on two important parameters: the processing gas flow $\Gamma_{C_2H_2}$ and the duty cycle D. The dust generation rate G_d is obviously proportional to D and the amount of processing gas density available in the plasma, which is determined by the C_2H_2 flow. Therefore G_d can be reasonably

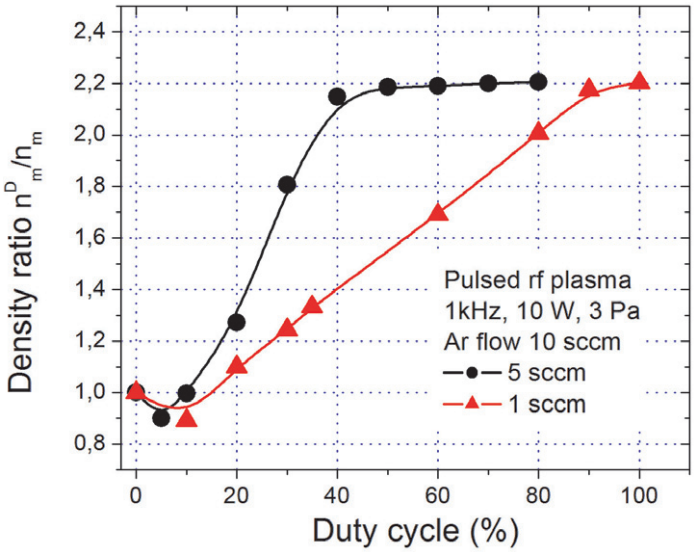

Figure 9. Metastable density ratio between dusty plasma and pristine plasma during the same duty cycle.

expressed as follows:

$$G_d = a_1 D \Gamma_{C_2H_2}, \tag{16}$$

where a_1 is a parameter that depends on the plasma power. In this consideration, since the plasma power was fixed at 10 W, a_1 is considered to be constant.

The loss rate L_d of dust particles is roughly proportional to the off time of the plasma when the particles lose their charge and some of them can escape to the chamber wall. L_d is therefore inversely proportional to the duty cycle. Meanwhile, L_d linearly depends on the dust particle density n_d since the uncharged dust is mainly driven out by diffusion in collision with background gas. Thus L_d can be written as

$$L_d = \frac{a_2 n_d}{D}. \tag{17}$$

Similar to a_1, a_2 is also a constant with fixed plasma power. In steady state conditions, the two rates are equal ($L_d = G_d$) giving the confined dust density. Combining equations (16) and (17), we obtain the relation for the confined dust density in a pulsed rf plasma:

$$n_d = \frac{a_1}{a_2} \Gamma_{C_2H_2} D^2. \tag{18}$$

However, interpretation of results in the case of a pulsed rf discharge is not as straightforward as in the continuous discharge. In order to compare measured metastable densities of plasmas at different duty cycles, one has to adopt a new quantity, which is the density ratio of dusty to pristine plasmas at the same duty cycle and plasma condition. This ratio is representative of the dust population in the pulse modulated dusty plasma. The relation of density ratio to the duty cycle of dusty plasmas prepared by two different acetylene flows (5 and 1 sccm) is expressed in figure 9. As already mentioned, the metastable density depends on the balance between two opposing effects of the dust particles. The loss of metastable atoms on the dust particle surface is linearly proportional to the dust density. The metastable excitation rate is, however,

exponentially proportional to the electron temperature [29], which more or less quadratically depends on the charge portion on the particles [40]. According to equation (18), with an increase in duty cycle the density of confined dust should increase quadratically. The metastable density ratio, however, should start from unity and decrease to a shallow minimum before increasing to a plateau at larger duty cycles (figure 9).

The plateau appearing at larger duty cycles is a consequence of the close parking effect, which reduces the particle charge when particles are too close to each other. The close parking effect becomes important at high particle density. With increasing dust density, the charge portion, and thus metastable density, cannot increase any further. The saturation occurs at 40% for the 5 sccm and at 90% for the 1 sccm gas flows, respectively (figure 9). The dust density of these two plasmas as calculated from equation (18) is relatively equal ($8100a_1/a_2$ for the 1 sccm case at 90% duty cycle and $8000a_1/a_2$ for the 5 sccm case at 40% duty cycle), which confirms our estimation of confined dust density in pulse modulated plasmas.

5. Conclusions

Argon metastable density was measured in rf plasmas and compared with a simple model for metastable density. The model can explain the trend of the metastable density with respect to the change of plasma input power. In order to apply this model to the case of dusty plasmas, the excitation channel by cascades from higher levels has to be taken into account.

The metastable density responds closely to the time evolvement of the dust growth in the processing plasma. From the temporal behavior of metastable density, we can identify the times T_{trans}, T_{void} and T_{p} for the α–γ' transition, the appearance of the dust void and the dust particle growth period, respectively. The metastable density can be used as an indicator of the changes in the plasma, especially electron temperature and density as well as to trace the phase transitions in a processing plasma between: nucleation, agglomeration, accretion and dust-expelling phases.

The change in the metastable density of dusty plasmas in comparison with that of pristine plasmas is the result of the balance between two effects depending on dust particle size and density: the loss of metastable atoms due to quenching at the dust particle surfaces and the increase of the excitation rate due to the increase of the electron temperature. In a void-free dust dense plasma, the metastable density is much higher in a dusty plasma than in a pristine plasma since the electron temperature in this plasma is significantly increased. Meanwhile, at low dust density, the loss effect can outweigh the enhancement effect. The metastable density in the dusty plasma therefore is lower.

By comparing the metastable density in a dusty plasma with different dust sizes and densities produced by hydrocarbon-containing plasmas, one can conclude that

1. The dust particle radius growth rate after the α–γ' transition in a hydrocarbon-containing plasma is proportional to $t^{-1/2}$, which is the combination of neutral and ionic growths.
2. The confined dust density in a pulsed processing plasma is proportional to the processing gas flow and to the square of duty cycle.

Through measuring the metastable density, TDLAS therefore can be used as an indirect tool to study the dust growth process in processing plasmas.

Acknowledgments

This work was supported by the Deutsche Forschungsgemeinschaft through SFB/TR 24. One of us (HTD) gratefully acknowledges the receipt of an International Max Planck Research School for Bounded Plasmas fellowship granted by the German State of Mecklenburg-Vorpommern.

References

[1] Melzer A and Goree J 2008 Fundamentals of dusty plasmas *Low Temperature Plasmas* vol 1 ed R Hippler, H Kersten, M Schmidt and K H Schoenbach (Berlin: Wiley-VCH) p 129
[2] Hippler R and Kersten H 2008 Applications of dusty plasmas *Low Temperature Plasmas* vol 2 ed R Hippler, H Kersten, M Schmidt and K H Schoenbach (Berlin: Wiley-VCH) p 787
[3] Selwyn G S, McKillop J S, Haller K L and Wu J J 1990 *J. Vac. Sci. Technol.* A **8** 1726
[4] Bouchoule A (ed) 1999 *Dusty Plasmas: Physics, Chemistry and Technological Impacts in Plasma Processing* (New York: Wiley)
[5] Stoffels E, Stoffels W W, Kersten H, Swinkels G H P M and Kroesen G M W 2001 *Phys. Scr.* T **89** 168
[6] Law D A, Tomme E B, Steel W H, Anaratonne B M and Allen J E 1999 *Proc. 24th Int. Conf. on Phenomena in Ionized Gases —ICPIG 1999 (Warsaw, Poland)* vol 4 p 109
[7] Swinkels G H P M, Kersten H, Deutsch H and Kroesen G M W 2000 *J. Appl. Phys.* **88** 1747
[8] Kersten H, Deutsch H, Stoffels E, Stoffels W W and Kroesen G M W 2003 *Int. J. Mass Spectrom.* **223–224** 313
[9] Selwyn G S, Singh J and Benett R S 1988 *J. Vac. Sci. Technol.* A **7** 2758
[10] Bouchoule A 1993 *Phys. World* **6** 47
[11] Do H T, Thieme G, Fröhlich M, Kersten H and Hippler R 2005 *Contrib. Plasma Phys.* **45** 1–8
[12] Barnes M S, Keller J H, Forster J C, O'Neill J A and Coultas D K 1992 *Phys. Rev. Lett.* **68** 313–6
[13] Boufendi L and Bouchoule A 1994 *Plasma Sources Sci. Technol.* **3** 262–7
[14] Stefanovic I, Scharwitz C, Kovacevic E, Berndt J and Winter J 2008 *IEEE Trans. Plasma Sci.* **36** 1018–9
[15] Fridman A A, Boufendi L, Hbid T, Potapkin B V and Bouchoule A 1996 *Appl. Phys.* **79** 1303–14
[16] Martin W C *et al NIST Atomic Spectra Database* (Gaithersburg, MD: National Institute of Standards and Technology) http://physics.nist.gov/PhysRefData/ASD/
[17] Wolter M, Do H T, Steffen H and Hippler H 2005 *J. Phys. D: Appl. Phys.* **38** 2390–5
[18] Olejnicek J, Do H T, Hubicka Z, Hippler R and Jastrabik L 2006 *Japan. J. Appl. Phys.* **45** 8090–4
[19] Kersten H, Wiese R, Thieme G, Fröhlich M, Kopitov A, Bojic D, Scholze F, Neumann H, Quaas M, Wulff H and Hippler R 2003 *New J. Phys.* **5** 93
[20] Matyash K, Fröhlich M, Kersten H, Thieme G, Schneider R, Hannemann M and Hippler R 2004 *J. Phys. D: Appl. Phys.* **37** 2703
[21] Kersten H, Thieme G, Fröhlich M, Bojic D, Tung D H, Quaas M, Wulff H and Hippler R 2005 *Pure Appl. Chem.* **77** 415–28
[22] Do H T, Kersten H and Hippler R 2008 *New J. Phys.* **10** 053010
[23] Kersten H, Stoffels E, Stoffels W W, Otte M, Csambal C, Deutsch H and Hippler R 2000 *J. Appl. Phys.* **87** 3637–45
[24] Tatanova M, Thieme G, Basner R, Hannemann M, Golubovskii Yu B and Kersten H 2006 *Plasma Sources Sci. Technol.* **15** 507
[25] Demtröder W 2000 *Laserspektroskopie* (Berlin: Springer)
[26] Scheibner H, Franke S, Solyman S, Behnke J F, Wilke C and Dinklage A 2002 *Rev. Sci. Instrum.* **73** 378
[27] Czerwiec T and Graves D B 2004 *J. Phys. D: Appl. Phys.* **37** 2827–40
[28] McMillin B K and Zachariah M R 1995 *J. Appl. Phys.* **77** 5538–44
[29] Baisova B T, Strunin V I, Strunina N N and Khudaibergenov G Zh 2003 *Tech. Phys.* **48** 969–71
[30] Bogaerts A, Gijbels R and Vlcek J 1998 *J. Appl. Phys.* **84** 121–36

[31] Tachibana K 1986 *Phys. Rev.* A **34** 1007–15
[32] Yanguas-Gil A, Cotrino J and Alves L L 2005 *J. Phys. D: Appl. Phys.* **38** 1588–98
[33] Riccardi C, Barni R, Fontanesi M and Tosi P 2000 *Czech. J. Phys.* **50** S3
[34] Turner M M, Doyle R A and Hopkins M B 1993 *Appl. Phys. Lett.* **62** 3247–49
[35] Brzobohatý O and Trunec D 2005 *Proc. 14th Annu. Conf. of Doctoral Students — WDS 2005 (Prague, 7–10 June 2005) Part II* (for Physics of Plasmas and Ionized Media) pp 306–12 http://www.mff.cuni.cz/veda/konference/wds/contents/wds05.htm#ppm
[36] Haaland P, Garscadden A and Ganguly B 1996 *Appl. Phys. Lett.* **69** 904–7
[37] Boufendi L and Bouchoule A 2002 *Plasma Sources Sci. Technol.* **11** A211–8
[38] Dorier J L, Hollenstein Ch and Howling A A 1994 *J. Vac. Sci. Technol.* A **13** 918–26
[39] Strunin V I *et al* 2002 *Zh. Tekh. Fiz.* **72** 109
Strunin V I *et al* 2002 *Tech. Phys.* **47** 760 (Engl. Transl.)
[40] Hori Y, Ostrikow K, Toyoda H and Sugai H 2001 *Proc. XXV Int. Conf. on Phenomena in Ionized Gases (Nagoya, Japan, 17–22 July 2001)* vol 3 pp 25–6